

Topographic expressions of lunar graben

Melanie B. Callihan* and Christian Klimczak

STRUCTURAL GEOLOGY AND GEOMECHANICS GROUP, DEPARTMENT OF GEOLOGY, UNIVERSITY OF GEORGIA, ATHENS, GEORGIA 30602, USA

ABSTRACT

Graben, defined as landforms produced by normal faulting, have long been recognized on the Moon, but their map patterns, as well as topographic expressions, have not been studied systematically. The topography across graben and its along-strike variations reveal details about the growth of the normal faults forming the graben. Individual normal faults grow in length by the propagation of fault tips during slip events, which can also enlarge the displacement along the fault plane. Displacement and length accumulate and grow larger over time with more slip events, fault interaction, and linkage. We measured fault lengths and vertical offsets and then calculated the displacement for lunar graben using data from the camera and laser altimeter onboard the *Lunar Reconnaissance Orbiter*. Our study systematically investigated 14 graben systems across the lunar surface. Graben lengths were found to range from ~43 to 453 km, and displacements ranged from ~127 to 1115 m. These displacements were plotted against graben fault length to produce slip distributions, which revealed growth patterns involving mechanical interaction and fault linkage. Displacement-to-length scaling was used to further study the evolution of graben-bounding normal faults. We observed a sublinear growth pattern for lunar graben-bounding normal faults, consistent with growth of faults via segment linkage, where different stages of linkage are present on the lunar surface. Lunar graben-bounding faults show higher scaling ratios than previously estimated, likely due to variations in host-rock properties and mechanical stratigraphy.

LITHOSPHERE; v. 11; no. 2; p. 294–305; GSA Data Repository Item 2019082 | Published online 31 January 2019

<https://doi.org/10.1130/L1025.1>

INTRODUCTION

Planetary bodies lacking major erosional processes and atmospheres, such as the Moon, preserve the morphologies and topographic expressions of major landforms over long time scales. This enables us to study faults in terms of their lateral extent, segmentation, offset, fault displacement, and overall fault evolution. In recent years, the collection of high-resolution topographic measurements from the Lunar Orbiter Laser Altimeter (LOLA; Smith et al., 2010) on board the *Lunar Reconnaissance Orbiter* (LRO) gathered the data essential to create an in-depth understanding of lunar faults and structures. Using lunar graben geomorphology, geometry, displacement-to-length scaling, and overlap-to-spacing ratios, this study aimed to create a better understanding of the growth of graben-bounding normal faults on the Moon.

Graben Geomorphology

Normal faults, inclined planar discontinuities along which extensional strains are accommodated via frictional sliding, are commonly found across the surface of the Moon (Golombek, 1979; Hiesinger and Head, 2006; Smith et al., 2010; Watters and Johnson, 2010; Klimczak, 2014; Nahm, 2016). Graben are linear landforms marked by multiple, oppositely dipping (antithetic) normal faults that create a down-dropped block in the center (Fig. 1; Schultz et al., 2007; Fossen, 2009). Each displacement along a normal fault can be decomposed into its horizontal and vertical displacement components, heave and throw, respectively. Displacement is the total

offset considering horizontal and vertical movement (Fig. 1), and it can be calculated using the fault dip and throw, or it can be measured along slip. Graben that show similar offset on both faults are symmetric. Frequently, however, the two graben-bounding faults show differences (asymmetry) in displacement, where the fault with the higher displacement is considered the master fault, and the fault with lower displacement is the antithetic fault. The symmetry of a graben reveals information about its maturity. Asymmetric graben or half graben typically indicate the early stages of graben development, but as they grow larger, they become more symmetric.

Generally, fault growth is governed by preexisting discontinuities, the local or regional stress field, rock strength, and pore-fluid pressure (Arthur et al., 1963). Faults generally grow by accumulation of seismic slip (Walsh and Waterson, 1987; Cowie and Scholz, 1992a, 1992b) and fault linkage (Peacock and Sanderson, 1991; Cartwright et al., 1995; Mansfield and Cartwright, 2001). Isolated faults grow via continued slip events and enable the formation of fault populations, where groups of smaller faults occur in the same region. In the second case, faults can increase their length and displacement over time by linking or coalescing with other smaller faults in the region (Cartwright et al., 1995). These arrays of subparallel (en echelon) small faults consist of fault segments rather than one single fault slip plane and form different characteristic structures in map and outcrop view (Willemse, 1997; Fossen et al., 2010). When two faults grow toward one another, they begin to mechanically interact (Peacock and Sanderson, 1991; Willemse, 1997; Gupta and Scholz, 2000; Peacock, 2002; Soliva and Benedicto, 2005). Two segmented faults that approach another, but that are not physically linked, are said to underlap. Underlap reaches a critical point when fault segments and their stress fields start to interact with each other (Willemse, 1997). When fault tips have moved past one another, the faults are considered to be overlapping. Once

Melanie B. Callihan  <http://orcid.org/0000-0002-3314-5172>

*Corresponding author: melanie.callihan@uga.edu

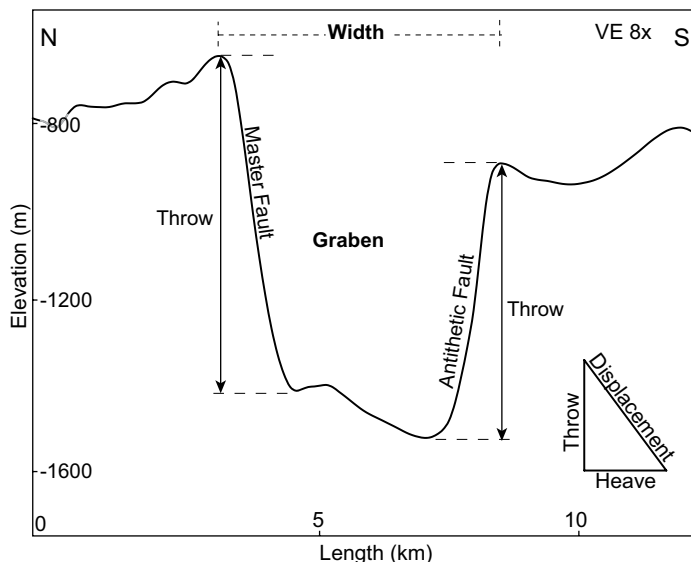


Figure 1. Topographic profile with eight times vertical exaggeration (VE) across a graben forming Rima Ariadaeus. Graben showing identified master and antithetic faults based on amount of throw/displacement.

interaction and linkage between segments begin, the fault tip propagation will temporarily arrest, and fault tips begin curving toward each other (Peacock and Sanderson, 1991; Willemse, 1997; Fossen and Rotevatn, 2016). Overlapping segments and underlapping segments are considered to be soft-linked when individual faults mechanically interact but do not form a continuous fault plane. Once the faults fully coalesce to form a single fault plane, the two original fault segments are considered hard-linked and can be identified by jogs or abrupt changes in fault orientation in map view (Willemse, 1997; Soliva and Benedicto, 2004). Graben that have grown by linkage of smaller segments as opposed to growth of a single isolated fault exhibit a much more complex set of structures and variety of map patterns. These map patterns show changes in spacing, overlap, and sudden changes in fault strike. Spacing is defined as the horizontal distance between two fault surfaces, whereas the overlap is the distance between the two individual overlapping fault tips.

To better understand fault growth, slip distributions have been used to analyze the way in which the fault geometry varies with length and to describe the relationship between displacement and fault length. A slip distribution highlights changes in displacement along the fault length, which, in a single fault, shows a gradual increase in displacement from the fault tip to the fault center. The maximum displacement is typically located in the center of the fault trace. The general shape of the slip distributions can vary from peaked to more flattened or plateaued profiles. In cases where more than one fault is involved, slip distributions can reveal linked or interacting faults with respectively higher displacements that skew toward one another. Fault growth via segment linkage is reflected in their slip distributions. Plateaued slip distributions arising from linked segments can indicate an intermediate stage of fault growth, whereas peaked slip distributions can indicate early or more advanced stages of fault growth (Peacock and Sanderson, 1991; Cartwright et al., 1995; Kim et al., 2004). Our analysis reveals how displacement changes with fault length, how lunar faults mechanically interact, and how that affects the shape and magnitude of a slip distribution. Additionally, the slip distributions and scaling allow us to infer information about the mechanical rock

properties and regional stresses (Cowie and Scholz, 1992b) for future research on lunar normal faults.

Previous studies suggested that maximum displacement (D_{\max}) and fault length (L) are related to one another by:

$$D_{\max} = \gamma L^c, \quad (1)$$

where γ is a constant dependent on rock type and regional stresses (Cowie and Scholz, 1992b), and c is the scaling exponent. In scenarios where faults are isolated, the scaling exponent was found to be near unity, whereas the effect of fault linkage or restriction at depth resulted in lower exponents. Previous studies on faults have revealed D_{\max}/L (γ) ratios of ~0.001–0.05 (Muraoka and Kamata, 1983; Walsh and Watterson, 1987; Krantz, 1988; Opheim and Gudmundsson, 1989; Peacock and Sanderson, 1991; Cowie and Scholz, 1992a; Dawers et al., 1993; Cartwright et al., 1995; Dawers and Anders, 1995; Clark and Cox, 1996; Watterson et al., 2000; Mansfield and Cartwright, 2001; Schultz and Fossen, 2002; Schultz et al., 2006; Polit et al., 2009; Watterson and Johnson, 2010; Gudmundsson et al., 2013; Roggon et al., 2017).

Graben on the Moon

The majority of graben on the Moon occur along the periphery of the lunar maria (Fig. 2A; Golombek and McGill, 1983; Watterson and Johnson, 2010; Nahm, 2016), but they are also found in floor-fractured craters (Schultz, 1976; Jozwiak et al., 2012, 2015), in large impact basins (Wilhelms et al., 1979; Nahm, 2016), and on very local scales (Watterson et al., 2000; Watterson and Johnson, 2010; French et al., 2015). Graben occur in a variety of terrains, including basaltic mare, anorthositic highlands, and in mare-highland transitions. The majority of graben analyzed in this study were found at the mare-highland transitions and in Schrödinger basin (Figs. 2B and 2C).

Large-scale lunar graben have not yet been systematically investigated for their along-strike characteristics in order to fully understand their geomorphologic expressions. Our investigation examines these relationships and thus reveals growth mechanisms involving fault linkage and interaction and their displacement-to-length scaling relationships. Previous studies have investigated smaller lunar graben for geomorphological patterns (Watterson and Johnson, 2010), and an in-depth study of an isolated lunar normal fault was conducted (Nahm and Schultz, 2015). Theoretical D_{\max}/L ratios for lunar faults are predicted to scale at 0.001 due to the influence of the low lunar surface gravitational acceleration (Schultz et al., 2006). None of these previous studies considered the slip distributions, D_{\max}/L scaling, or overlap-to-spacing relationships of normal faults in large and segmented graben systems.

Graben formation on the Moon has been a long-standing topic of discussion, and it has been suggested that their formation may be linked to the intrusion of dikes (Head and Wilson, 1993; Wilson et al., 2011; Klimczak, 2014) or due to extension associated with sites of prominent positive gravity anomalies, so-called mascon basins (Solomon and Head, 1979; Freed et al., 2001). The methodology used in this research does not directly allow us to distinguish among graben formation mechanisms, but it does enable us to characterize the growth of the graben-bounding faults with implications for mechanical properties of the lunar lithosphere. For that, we present a detailed examination of 14 different graben systems (Fig. 2B). Slip distributions were generated for these graben by measuring and plotting the displacements along the lengths of both graben-bounding faults. Slip distributions that incorporate both graben-bounding faults reveal maximum displacements, allow for comparison of displacements between the two opposing faults, and thus facilitate assessments of graben symmetry. The overall shapes of slip distributions are also useful for understanding

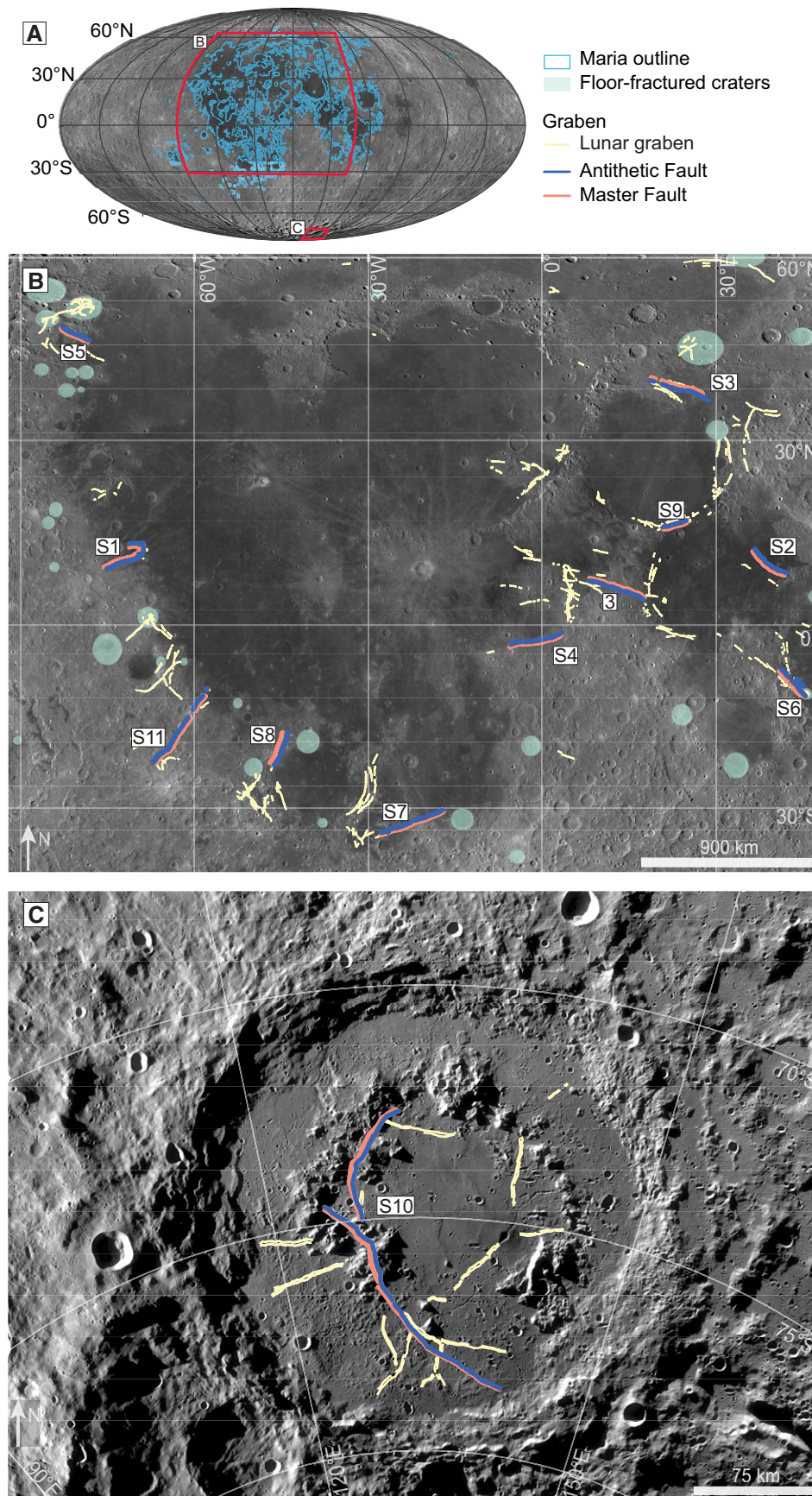


Figure 2. Overview of the study areas. (A) Location of the subset images (red outline) relative to the maria on the lunar nearside (blue outline). (B) Lunar Reconnaissance Orbiter Camera (LROC) mosaic in equirectangular projection showing all individual graben locations mapped in this study (yellow lines). Our specific study sites around the lunar maria highlight the master (orange line) and antithetic (blue line) graben-bounding faults. Individual figures (labeled in white boxes) can be found in the Data Repository Item (see text footnote 1). Floor-fractured craters containing graben are distributed widely (green shading). (C) LROC mosaic in south polar orthographic projection of Schrödinger basin with mapped graben.

subsurface geology or fault interaction. The well-exposed and preserved graben-bounding faults allow us to use D_{\max}/L scaling to interpret fault evolution and investigate the possibility of multiple graben fault populations.

MATERIALS AND METHODS

Graben-bounding normal faults in this study were identified using a combination of the Lunar Reconnaissance Orbiter Camera (LROC) global mosaic, with a resolution of 100 m/pixel, and the 118 m/pixel digital elevation model (DEM) from LOLA (e.g., Fig. 3A). Throw measurements obtained from the LOLA DEMs were manually extracted in ArcGIS 10.2 using the 3D Analyst toolbox.

Mapping of faults and fault segments was conducted in several stages. The first stage consisted of identifying and mapping fault traces, and this was followed by the extraction of elevation data along the normal fault traces (Figs. 3A and 3B). In order to collect accurate and coherent data, geodetic fault lengths were measured along the map trace of the fault, terminating in the fault tips. If graben-bounding faults appeared in several en echelon faults, we measured the length and trace of all interacting faults. When en echelon fault segments met in an overlap (Willemse, 1997), we discontinued the fault trace and mapped two individual faults. In cases where graben were superposed by impact craters or pits, fault traces were terminated, and a new segment was started. When the fault was superposed by features such as ejecta blankets, we mapped the fault as inferred. All geologic features were mapped at the highest resolution of the data. Figure 3B shows an example of one of the resulting structural maps with all geologic features considered. Once mapping was complete, the map patterns were interpreted for fault growth.

We extracted topographic profiles (Fig. 1) from the LOLA DEMs across each of our studied graben in evenly spaced intervals (see position of one such topographic profile in Fig. 3A). The interval of spacing of profiles was determined based on fault length in order to create a consistent representation each fault segment. On average, these profiles were spaced in 2–5 km intervals, with larger intervals ranging up to 8 km and the smallest segments having profiles spaced at <1 km intervals. Topographic profiles ranged in length from 20 to 30 km to ensure that graben topography and local topographic variations would be appropriately identified. For each profile, we identified the locations of graben-bounding faults (Fig. 1) to determine their throw. Throw measurements can be converted into the true fault displacement if the slip direction and fault dip are known. We assumed fault motion to be pure dip slip and fault dips to be 60°.

Finally, slip distributions for each graben were derived by plotting the calculated true displacement along the map trace for each graben-bounding fault segment (Fig. 3C). We also determined the master and antithetic faults for each graben system (Fig. 1) and assessed the amount and location of the displacement maximum along the slip distribution (Fig. 3C). We assigned the master fault upon visual inspection of our slip distributions to the fault with the maximum displacement along the total graben fault trace (Figs. 2B, 2C, 3B, and 3C). When maximum displacements were too similar for both graben fault traces, we assigned the master fault to the fault with the higher displacement average. Both the maximum displacement and length values for each fault segment were extracted from the data for our fault scaling analysis.

RESULTS

Map Patterns and Slip Distributions

Similar to previous studies (Wilhelms et al., 1979; Watters and Johnson, 2010; Nahm, 2016), we surveyed the LROC base map and mapped

all graben that could be clearly identified on the scale of this data set. We found that lunar graben are commonly segmented, and 1800 normal fault segments were recognized and mapped in this study. From this population, we then selected 14 different study sites for detailed characterization of the graben-bounding normal faults. The graben investigated in this study are described individually in the GSA Data Repository Item¹ and are summarized in Table 1. These graben include Rima Ariadaeus (Fig. 3), Rima Cardanus (two structures; Data Repository Fig. S1), Rima Cauchy (Fig. S2), Rimæ Daniell (Fig. S3), Rima Flammarion and Oppolzer (Fig. S4), Rimæ Gerard (Fig. S5), Rimæ Goclenius (two structures; Fig. S6), Rima Hesiodus (Fig. S7), Rimæ Mersenius (Fig. S8), Rimæ Plinius (Fig. S9), the graben in Schrödinger basin (Fig. S10), and Rimæ Sirsalis (Fig. S11).

The graben presented in this study display a wide range of map patterns and morphologies and cannot be classified into specific populations based on their structural characteristics. In the following, we first summarize overall observations and then discuss findings on the slip distributions from topographic measurements.

Grabens were found in multiple terrain types (Table 1), including highlands, mare, and the transitional boundaries between them. Graben trends listed in Table 1 show a wide range of orientations, and when graben were in spatial association with the maria, they preferentially showed orientations concentric or radial to these units. The fault systems comprising the graben ranged in length from ~43 to 453 km. Maximum displacements for the analyzed 14 graben ranged from 128 to 1115 m, with an average maximum displacement of 444 m. We also categorized dip direction of the master fault (Table 1) for later interpretation (see implications for origin of graben). Graben widths were measured for each graben and also compiled in Table 1. Their maximum widths ranged from 1 to 5 km. Grabens were also assessed in terms of their cross-sectional symmetry, with structures showing symmetric, asymmetric, and variable geometries (Table 1).

Graben include highly segmented faults as well as structures composed of long, single segments for both master and antithetic faults, ranging from 2 to 32 individual segments. The analyzed graben contained a total of 184 individual fault segments with individual fault lengths ranging from 3 to 166 km (Table 1). Rima Cardanus 1 (Fig. S1) and Rimæ Plinius (Fig. S9) are the only graben that are composed of two single oppositely dipping normal faults; all other systems showed varying amounts of fault segmentation (Table 1).

All 14 graben systems show a high variability in the types of segment interaction and linkage. Nine systems display at least one overlapping (i.e., soft-linked) fault segment, and many display more than three such overlap map patterns. Underlap between individual fault segments was found to occur for fault segments at Rima Flammarion and Oppolzer (Fig. S4), Rimæ Gerard (Fig. S5), Rimæ Goclenius 1 (Fig. S6), Rima Hesiodus (Fig. S7), and the graben in Schrödinger basin (Fig. S10). Fault jogs (i.e., hard-linked) were predominantly found in graben systems that also hosted overlapping or underlapping fault segments.

The fault throws and their resulting slip distributions for each graben in this research also display a wide range of displacement amounts and overall slip distributions along the fault strike. From all of our detailed slip distributions (Fig. 3; Figs. S1–S11 [see footnote 1]), we compiled the general shapes of the master fault to better understand differences in slip distribution and to further classify them based on their shapes (Fig. 4). We extracted the profile shape by removing information on the individual faults to capture the overall slip distribution shape. These generalized slip

¹GSA Data Repository Item 2019082, detailed descriptions of graben investigated in this study, including maps and slip distribution diagrams, full descriptions of map patterns, fault segmentation, and fault linkage, as well as categorization of the slip distributions, is available at <http://www.geosociety.org/dataproxy/2019/>, or on request from editing@geosociety.org.

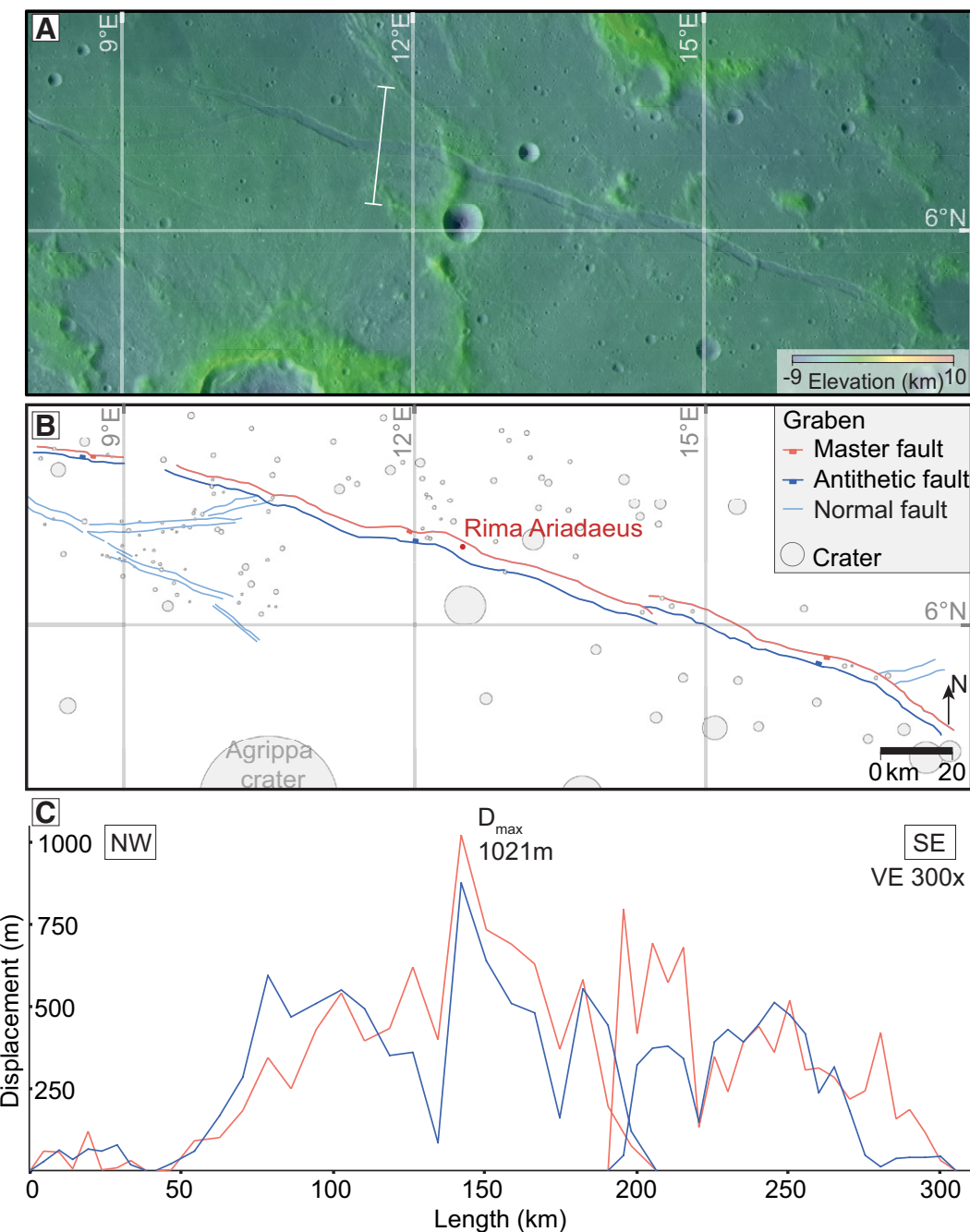


Figure 3. Structural analysis of Rima Ariadaeus centered at 12°N, 007°E. (A) Lunar Orbiter Laser Altimeter (LOLA) digital elevation model (DEM) overlaid on Lunar Reconnaissance Orbiter Camera (LROC) global mosaic in equirectangular projection, showing the extent of the graben and individual faults. The white line indicates where part of the topographic profile shown in Figure 1 was extracted. (B) The structural map of the region shown in A highlighting six individual fault segment traces and surrounding features. We produced the structural maps based on this methodology for all 14 graben systems. (C) Topographic profiles were then used to create slip distributions along strike of the graben. The interpreted slip distributions for this graben reveal a peak in displacement at the center of the graben length. The legend presented here applies to all figures in the Data Repository Item (see text footnote 1).

TABLE 1. GRABEN ANALYZED FOR THIS STUDY

Graben	Location	Terrain type	Graben trend	Length (km)	D_{\max} (m)	Master fault scarp	Max. graben width (km)	Graben symmetry	Fault segments (n)	Fault segment lengths (km)	Slip distribution D_{\max}/L ratio	Figure number*
Rimæ Ariadaeus	12°N, 007°E	Highlands	WNW/ESE	304.8	1022.0	South-dipping	5.4	Symmetric	6	29–162	0.0034	3
Rimæ Cardanus 1	13°N, 069°W	Transition	E/W	72.5	168.5	North-dipping	2.5	Symmetric	2	72.5	0.0023	S1
Rimæ Cardanus 2	11°N, 071°W	Transition	SW/NE	223.2	302.5	South-dipping	2.8	Symmetric	10	25–104	0.0014	S1
Rimæ Cauchy	10°N, 038°E	Mare	NW/SE	204.8	200.2	North-dipping	2.7	Asymmetric	20	9–44	0.0010	S2
Rimæ Daniell	38°N, 45°E	Transition	NW/SE	264.7	272.4	South-dipping	3.5	Asymmetric	32	3–32	0.0010	S3
Rimæ Flammarion and Oppolzer	02°S, 001°W	Highlands	WSW/ENE	282.9	313.5	North-dipping	3.3	Symmetric	9	10–166	0.0011	S4
Rimæ Gerard	46°N, 080°W	Transition	NW/SE	115.3	538.3	North-dipping	2.2	Symmetric	4	18–97	0.0047	S5
Rimæ Goclenius 1	08°S, 043°E	Mare	NW/SE	179.3	291.4	North-dipping	3.3	Variable	22	3–43	0.0016	S6
Rimæ Goclenius 2	09°S, 044°E	Mare	NW/SE	42.9	127.5	North-dipping	2.0	Asymmetric	6	6–19	0.0030	S6
Rimæ Hesiodus	31°S, 022°W	Transition	NE/SW	303.7	381.4	North-dipping	4.7	Symmetric	30	4–91	0.0013	S7
Rimæ Mersenius	19°N, 046°W	Transition	NNE/SSW	173.0	348.7	East-dipping	3.4	Symmetric	5	28–112	0.0020	S8
Rimæ Mersenius	17°N, 023°E	Transition	WNW/ENE	121.2	388.9	North-dipping	3.4	Asymmetric	2	121.2	0.0032	S9
Schrödinger graben	75°S, 128°E	Basin	NNW/SSW	234.1	1115.2	East-dipping	3.7	Variable	8	9–106	0.0048	S10
Rimæ Sirsalis	16°S, 059°W	Transition	SW/NE	453.3	752.6	West-dipping	4.1	Variable	28	3–90	0.0017	S11

*Figures S1–S11 are located in the GSA Data Repository item (see text footnote 1).

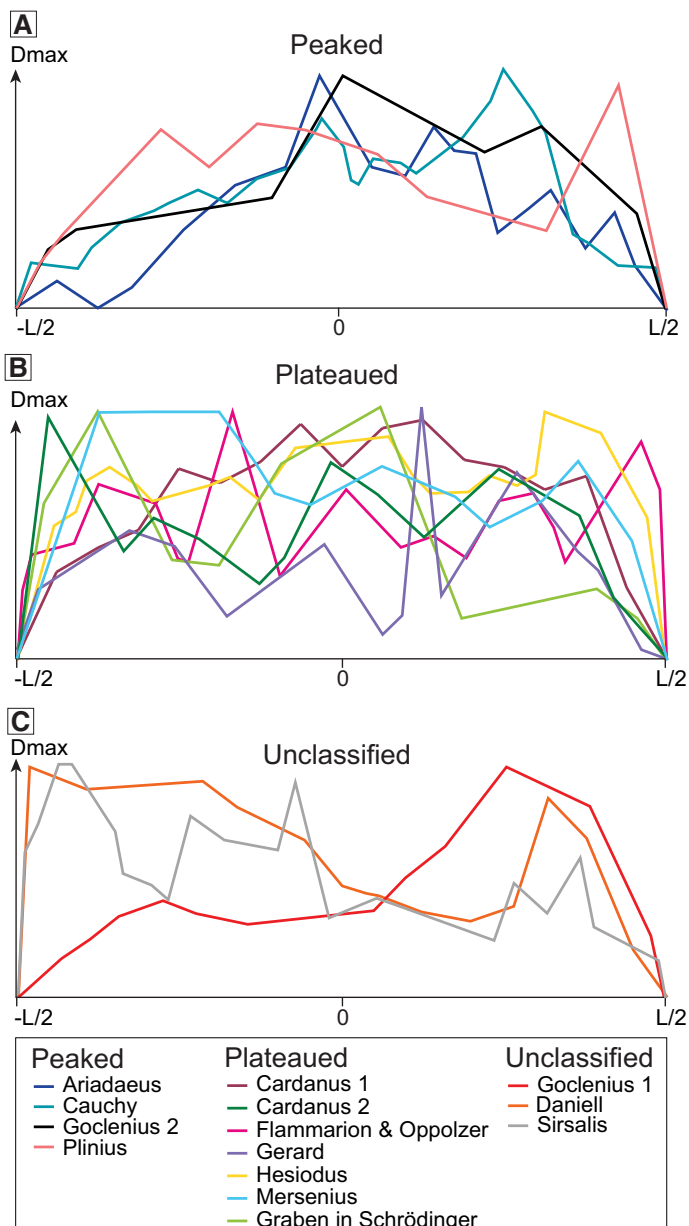


Figure 4. Slip distribution categories of all graben normalized by fault length (L) and displacement (D). (A) Peaked slip distributions highlight a general peak near the center along the graben fault length (0), tapering toward the tips ($-L/2$ and $L/2$). (B) Plateaued slip distributions reveal a much more flat-topped profile without a distinct central peak, which can likely be attributed to an intermediate stage of fault interaction. (C) Unclassified slip distributions do not clearly present either category and show a high variability in displacement.

distributions were then normalized for length and maximum displacement. This classification method reduces detail and allows us to better compare the general shapes of slip distributions for profiles composed of a single fault segment with profiles composed of 32 fault segments. Differences are still present in a number of segments and can be attributed to this decrease in detail. The individual slip distribution shapes for each graben display a much higher level of detail, as well as showing all individual fault segments (see Data Repository Item).

Our displacement distribution analysis allowed us to categorize Rima Ariadaeus (Fig. 3), Rima Cauchy (Fig. S2), Rimæ Goclenius 1 (Fig. S6), and Rimæ Plinius (Fig. S9) as having overall peaked slip distributions (Fig. 4A). Generally, the peaks for these slip distributions were located near the center of the entire fault length. Displacement variations toward the tips were attributed to the influence of rough terrain and/or fault interaction, as well as the generalization of profile shapes.

We classified the overall shapes of Rima Cardanus 1 and 2 (Fig. S1), Rima Flammarion and Oppolzer (Fig. S4), Rimæ Gerard (Fig. S5), Rimæ Hesiodus (Fig. S7), Rimæ Mersenius (Fig. S8), and the graben in Schrödinger basin (Fig. S10) as plateaued slip distributions (Fig. 4B). These slip distributions do not clearly indicate a single peak, but rather reflect small variations in displacement along a more constant slip distribution along the entire length of the graben. Unclassified slip distributions (Fig. 4C), such as Daniell (Fig. S4), Rimæ Goclenius 1 (Fig. S6), and Rimæ Sirsalis (Fig. S11), were graben that formed by a large number of individual fault segments (Table 1). These individual fault segments show a high variability of along-strike displacement (Fig. 4C), and they may be in various stages of fault interaction. Such stages of interaction were observed to include many overlapping segments with different amounts of maximum displacements, slip distributions of neighboring fault segments that show displacement maxima skewed toward one another, or multiple displacement maxima within one fault segment.

Among the 14 different graben, few displayed specific characteristics that stood out in our mapping and analysis. Graben located in rough or elevated terrain frequently showed high displacement along those regions. Both Rima Ariadaeus (Fig. 3) and the graben in Schrödinger basin (Fig. S10) had maximum displacements of 1022 m and 1115 m, respectively, where the graben perpendicularly crossed a ridge of rough terrain. Rough terrain or elevated topography also produced relatively high maximum displacements in Rimæ Sirsalis. Those displacements were the highest displacements measured in this study, exceeding typical maximum displacements by a factor of two or three (Table 1). In situations where the graben was oriented parallel to a mare unit, the master fault scarp faced (dipped toward) the mare (Fig. 2B). Rima Cardanus 1 (Fig. S1), Rimæ Daniell (Fig. S3), Rimæ Flammarion and Oppolzer (Fig. S4), Rimæ Hesiodus (Fig. S7), and Rimæ Plinius (Fig. S9) were all oriented circumferentially to their respective mare and displayed a master fault facing toward the mare center.

Displacement-to-Length Scaling

This study analyzed 14 predominantly segmented graben with a total of 184 individual faults. First, we investigated all fault segments, with their individual maximum displacements and fault segment lengths, followed by an analysis of the maximum displacement and length of the entire graben system.

Displacement-to-length (D_{\max}/L) scaling studies suggest a power-law relationship that depicts proportional growth of displacement and fault length (Cowie and Scholz, 1992a; Dawers et al., 1993; Clark and Cox, 1996; Schultz et al., 2006; Polit et al., 2009), which can reflect interaction and growth via fault linkage. Based on Equation 1, a scaling exponent $c =$

1 indicates a linear scaling law, whereas any other number indicates scale-dependent (γ) geometry. The D_{\max}/L scaling plot in Figure 5A displays a range of three orders of magnitude for the normal fault data from the 184 individual structures of this study. The data points are scattered broadly and indicate that fault displacements have grown disproportionately to length. Scatter in the data is attributed to location-specific controls, such as host-rock type, fault driving stresses, and/or layer thickness. Individual D_{\max}/L ratios range from 0.0012 to 0.135, with an average of 0.0121. Our regression analysis revealed a power-law relationship with a scaling exponent of $c = 0.45$ and a γ value of 1.82, indicative of sublinear fault growth. The great variability and poor fit of our D_{\max}/L data are apparent in the low R^2 value of 0.37.

We also evaluated the D_{\max} and total graben length for all 14 graben of our study in comparison to previously analyzed normal faults (Fig. 5B). Lunar fault length generally plots among the longest structures for which D_{\max}/L data have been compiled. The D_{\max}/L ratios fall between a γ of 10^{-2} and 10^{-3} and appear moderately scattered. The graben system D_{\max}/L ratios range from 0.0010 to 0.0048 (Table 1), with an average of 0.0023 and a median of 0.0018. Our regression statistics reveal a power-law relation of $D_{\max} = 0.17L^{0.64}$, with an R^2 value of 0.39.

Previously, D_{\max}/L ratios for the Moon were modeled by Schultz et al. (2006), which predicted lunar fault D_{\max}/L ratios approximately ~ 0.04 times those of terrestrial faults. Our results indicate that lunar graben fall slightly higher than the predicted D_{\max}/L ratio of ~ 0.001 (Schultz et al., 2006). A D_{\max}/L ratio of ~ 0.0036 was also previously determined from the average maximum displacement and length of six lunar graben ranging in length from 34 km to 127 km (Watters and Johnson, 2010), scaling similarly to our results. In comparison to examples of terrestrial normal faults (Muraoka and Kamata, 1983; Walsh and Watterson, 1987; Krantz, 1988; Opheim and Gudmundsson, 1989; Peacock and Sanderson, 1991; Dawers et al., 1993; Cartwright et al., 1995), lunar graben fault lengths are substantially longer than the compilation of terrestrial normal fault equivalents, and the displacement scales lower compared to examples from Earth.

Overlap and Spacing Analysis

To better understand fault growth and investigate the presence of multiple fault populations, we analyzed the regions where fault overlap occurred. We selected all fault segments that had a section of the fault trace overlap with another fault segment. We measured the spacing (separation) and the amount of overlap between 43 faults. The results of our overlap-to-spacing relationships are shown in a logarithmic plot, which reveals a wide range of fault overlap-to-spacing ratios (Fig. 5C). Observed normal fault spacing on the Moon occurs on the order of hundreds of meters to kilometers, whereas overlap shows variability across two orders of magnitudes, ranging from hundreds of meters to tens of kilometers. The statistical (power-law) fit of the overlap-to-spacing ratio is 5.88, with a scaling exponent of 0.45, and a low R^2 of 0.26. In comparison to the compilation of terrestrial overlap-to-spacing data by Long and Imber (2011), our data plot among the largest spacings and overlaps (Fig. 5D). Our data plot within the same order of magnitude and thus show similar overlap-to-spacing ratios as those from the terrestrial fault data, where overlap is ~ 3 to 3.6 times the spacing (Long and Imber, 2011; Fossen and Rotevatn, 2016).

IMPLICATIONS FOR GROWTH OF NORMAL FAULTS ON THE MOON

Slip distributions can reveal information on magnitude and distributions of offset along strike of a fault and, thus, have been used to gain a better understanding of the growth and evolution of individual fault systems and

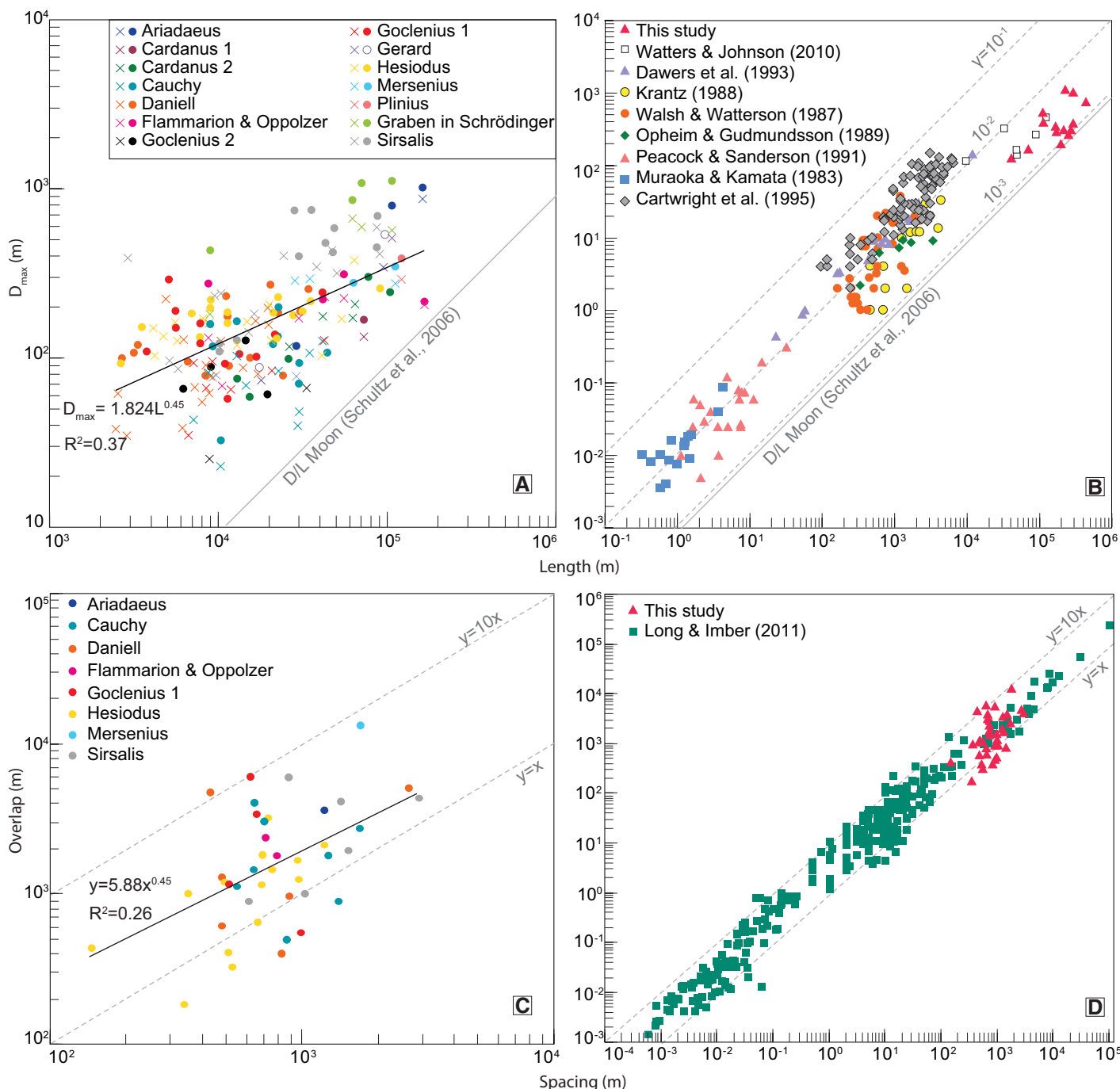


Figure 5. Displacement-to-length (D_{\max}/L) scaling and overlap-to-spacing data for lunar graben, where γ is a constant dependent on rock type and regional stresses (Cowie and Scholz, 1992b). (A) Displacement and length plotted for all fault segments (184) including master (solid circles) and antithetic faults (crosses). The plot shows measurements with respect to model prediction for lunar normal faults from Schultz et al. (2006). (B) Comparison of the master faults of this study (solid triangles) to a compilation of normal faults on Earth and previously derived data for the Moon. (C) Overlap-to-spacing plot for all overlapping fault segments of this study. (D) Comparison of overlap-to-spacing data with compilation of Long and Imber (2011).

fault populations (Cowie and Scholz, 1992a; Dawers and Anders, 1995; Willemse et al., 1996; Schultz and Fossen, 2002; Soliva et al., 2005). Specifically, slip distributions are commonly used as tools to understand driving stresses causing faulting, interaction, and linkage of fault segments, as well as detection of fault confinement within a mechanical stratigraphy. Furthermore, slip distributions are the only means by which accurate locations of maximum displacements for faults are determined, and thus they are a necessary tool for accurately determining and interpreting the displacement-to-length statistics. The D_{\max}/L ratio relationship is one of the most important methods for interpreting fault growth and possible host-rock properties. Additionally, overlap-to-spacing relationships of faults allow us to further interpret fault linkage and serve as a criterion to identify whether the investigated graben are part of a single or multiple fault populations.

Implications Arising from Slip Distributions

Among all analyzed graben, we observed the following trends among the slip distributions of the graben-bounding faults: (1) peaked slip distributions among all 14 graben, (2) certain faults with much higher displacements than the rest of their neighboring faults, (3) individual faults displaying skewed displacements in areas where they interact or link with other faults, (4) plateaued slip distribution profiles among all graben, and (5) variability in graben symmetry within all 14 graben.

Approximately half of the individual fault segments (Fig. S2C–11C) and isolated graben-bounding faults (Fig. S1C) were found to have peaked slip distributions. In individual faults, a peaked slip distribution indicates isolated or unrestricted fault growth. A peaked slip distribution for a graben system may also be caused by unrestricted fault growth and the lack of individual fault linkage. Most fault segments of our study showed peaked profiles, whereas only Rima Cardanus 1 (Fig. S1C), Rima Ariadaeus (Fig. 3C), Rimæ Goclenius 2 (Fig. S6), and Rima Cauchy (Fig. S2C) showed cumulative peaked profiles (for slip distributions of all segments added together).

Several faults in this study displayed skewed slip distributions. This can be observed for several segments within the slip distributions of Rima Ariadaeus (Fig. 3), Rima Cauchy (Fig. S2C), Rimæ Goclenius 1 (Fig. S6C), Rimæ Plinius (Fig. S9C), and Rimæ Sirsalis (Fig. S11C). These asymmetric slip distributions are frequently indicative of fault interaction, as displacements of two neighboring fault segments are observed to be skewed toward one another. This phenomenon is observed here in fault segments that overlap, overlap, or at hard-linked faults that have two or more throw maxima. Such asymmetry in slip distribution is caused by interacting and overlapping stress fields, resulting in localized higher displacements near another fault segment (Gupta and Scholz, 2000).

We identified seven graben where the entire slip distribution is plateaued (Fig. 4). These include Rima Cardanus (Fig. S1), Rimæ Flammarion and Oppolzer (Fig. S4), Rimæ Gerard (Fig. S5), Rima Hesiodus (Fig. S7), and Rimæ Mersenius (Fig. S8). The plateaued shapes of these graben systems can be attributed to abundant fault interaction or related to mechanical layer thickness. The plateaued slip distribution shape may also indicate fault restriction to a mechanical layer, causing the faults to grow in length while the depth of faulting and displacement are not increased (Soliva et al., 2005, 2006).

Our study found seven symmetric graben, four asymmetric graben, and three graben that show high variability within their symmetry (Table 1). Symmetry reveals information on maturity of the graben system. At the very first stage of graben formation, a single master fault is purely asymmetric due to the lack of another fault. A flexure of the layering toward the fault occurs, producing a rollover anticline. As fault growth continues, an antithetic fault is produced along the rollover anticline of

the master fault, and asymmetry decreases. Symmetric graben are interpreted as mature, as evident in their similar displacements across master and antithetic faults. Asymmetric graben, where antithetic and master fault displacements are found to be substantially different, are interpreted as less mature. The graben with variability in symmetry predominantly start out as asymmetric at the end of the graben system and become more symmetric along strike. This finding, and the fact that symmetric and asymmetric graben occur on the Moon, indicates that the timing and rate of tectonics involved in graben growth may have varied across the lunar surface, producing graben of various maturity stages. Additional evidence for that can be found in some asymmetric graben, such as Rima Daniell (Fig. S3), where there is a half graben.

Implications Arising from D_{\max}/L Scaling

The relationship between maximum displacement and fault length can reveal information on fault growth, interaction, and material properties of the host rock. Our analysis showed a wide range of D_{\max}/L ratios, which is likely related to fault system maturity and represents different stages of fault growth and linkage (Peacock and Sanderson, 1991; Walsh et al., 2002). It also showed that growth follows a sublinear path, indicating fault length accumulated faster than displacement. Isolated faults, which are somewhat rare (only two out of 14 graben systems in this study), account for the lowest D_{\max}/L ratios. Soft-linked faults are found to have higher displacements and lower length due to the temporary fault arrest (Willemse et al., 1996).

In contrast, hard-linked faults are found to show a high displacement and thus higher D_{\max}/L ratios. While soft-linked faults are present in nearly every graben system in this data set, hard-linked faults are present in only three systems and represent additional high displacement ratios. The D_{\max}/L statistic for this study shows a sublinear relationship with a lower D_{\max}/L ratio, indicating that fault lengths are disproportionately longer than their displacement. This can be tied to the abundance of plateau-shaped slip distributions, which are found to occur as one phenomenon of fault growth by segment linkage (Cartwright et al., 1995). This interpretation also correlates well with the observed overlap and spacing map patterns, indicating that long faults are mainly formed by linkage.

In comparison to terrestrial normal faults (Muraoka and Kamata, 1983; Walsh and Watterson, 1987; Krantz, 1988; Opheim and Gudmundsson, 1989; Peacock and Sanderson, 1991; Dawers et al., 1993; Cartwright et al., 1995), our data reveal the presence of longer faults yet similar D_{\max}/L ratios. Terrestrial faults used for a comparison are from different fault populations, yet they plot in a narrow region (Fig. 5B). The previously analyzed, smaller lunar graben-bounding normal faults and their respective D_{\max}/L ratios (Watters and Johnson, 2010) are comparable to the values revealed in our study. Our D_{\max}/L ratios plot above the calculated D_{\max}/L ratio proposed by Schultz et al. (2006; cf. Fig. 5B herein). The difference in scaling relations between our study and the predictions from Schultz et al. (2006) is likely due to the assumptions for their conceptual modeling. The scatter within our data set also may be attributed to the presence of multiple fault populations. Lunar normal faults may occur within one or multiple populations, which can be further distinguished with overlap-to-spacing ratios of interacting normal faults.

As described as part of the results, Rima Ariadaeus (Fig. 3), the graben in Schrödinger basin (Fig. S10), and Rimæ Sirsalis (Fig. S11) display much higher maximum displacements than other faults of this study. These higher maximum displacements correlate with rough terrain and with regions that have higher elevations. In contrast, graben located in smooth terrain generally have lower displacements. The graben contained in smooth mare or mare-highland transition zones show displacements

ranging between 169 and 538 m, whereas the graben located in rough highland terrain can show displacements upwards of 1000 m. Additionally, crosscutting of features with positive topography, such as rims of ancient craters, appear to cause an increase in the displacement of lunar graben-bounding faults. The influence of rough terrain on fault displacement may be linked to a change in mechanical properties or layer thickness in these areas. Rough or highland terrain may have mechanical properties or an increased layer thickness, both of which may lead to an increased fault displacement. Faults with lower displacement, located in smoother terrain, could by analogy reflect substantially different mechanical properties and/or a thinner mechanical layer than those found in the rougher highlands. Mechanical properties of the faulted lunar lithosphere and mechanical layering are further discussed in the next section.

Implications from Overlap and Spacing

Overlap-to-spacing ratios of faults can shed light on fault interaction and the presence of multiple fault populations. Our analysis of fault overlap and spacing among lunar normal faults revealed a wide range of these fault characteristics and their relationships to one another (Fig. 5C). This may be attributed to the diversity of lunar fault geomorphology. The average overlap-to-spacing ratio for our study was 5.5–6, which is higher than terrestrial equivalents. The average overlap-to-spacing ratio for all compiled terrestrial data sets is 3–3.5 (Long and Imber, 2011; Fossen and Rotevatn, 2016).

Generally, our data set of lunar graben faults plots within the range of terrestrial overlap-to-spacing ratios compiled by Long and Imber, (2011). The effect of surface gravitational acceleration that has been proposed to cause a lower D_{\max}/L scaling ratio for lunar faults (Schultz et al., 2006) is not apparent in the overlap and spacing relationships here (Fig. 5B). Thus, it can be deduced that overlap-to-spacing relationships of lunar normal faults behave similarly to terrestrial normal faults, and the scatter displayed in our data is due to similar reasons as that in the terrestrial data sets. Scatter in the data is attributed to location-specific controls, such as host-rock type, fault driving stresses, and/or layer thickness.

Mechanical layer thickness can be a strong factor controlling many aspects of a fault population, and previous observations have indicated a relationship exists between layer thickness and fault spacing. A characteristic fault spacing of ~0.5 times the layer thickness is found for fault populations on Earth (Soliva et al., 2006). Based on the layer thickness and spacing relationships proposed by Soliva et al. (2006), and under the assumption that this relationship can be extrapolated to faults on the Moon, our data reveal a layer thickness range of 0.5–5.8 km, with an average layer thickness of 1.86 km. Potential candidates for the layers that could be considered mechanical units are either the mare basalts or the megaregolith. Recent studies of the mare basalt thicknesses revealed ranges of 0.4–1.9 km (Michaut et al., 2016), 1.5–2 km along basin margins (Thomson et al., 2009), and 0.1–1.62 km, with some of the thickest sequences estimated at an average of 2.86 km (Gong et al., 2016) using various different types of methodologies.

The megaregolith thickness has equally been the subject of discussion, and previous estimates have varied widely. In recent studies, the megaregolith thickness has been suggested to range from ~100 km thick (Gillett et al., 2017) to more conservative estimates at 25 km, with a structural disturbance at ~10 km depth (Jaumann et al., 2012), and the presence of a 34–43 km thick highly fractured crust (Wieczorek et al., 2013). Based on these studies, the megaregolith is found to be much thicker than our estimate of mechanical layer thickness. This implies that the graben studied here are likely fully contained in a layer with rock-mechanical properties governed by those of the megaregolith, and thus it likely did not have a

direct impact on the variability of scaling behavior of the faults investigated here. However, the thickness estimates for mare basalts coincide to first order with the mechanical layer thickness range derived from fault spacing. Therefore, the mare basalts may have formed a mechanical layer that influenced the scaling properties of the graben-bounding normal faults.

Although the overlap-to-spacing relationships display scatter in the data, we did not detect any data clusters that would indicate if more than one normal fault population exists on the Moon or whether all normal faults are part of a single population. The scaling relationships derived in this study do not reveal if lunar normal faults are genetically linked to the same tectonic process or whether multiple tectonic processes could have formed them (see next section).

Implications for Origin of Graben

Our data show that lunar graben in spatial association with the maria show two preferred orientations with respect to them. Most commonly, they are either concentric or radial with regard to the nearest mare-filled basin. If a graben is concentric to a mare basin, we found that the master-fault dip direction points toward the mare unit, indicating that some lunar graben are closely tied to the emplacement of mare units or tectonics associated with basins and lowlands that are mare-filled. Most graben dissect the lunar maria and surrounding highlands around them, but no graben are found to be superposed by mare units. This is observed for Rima Hesiodus (Fig. S7), Rima Flammarion and Oppolzer (Fig. S14), Rimae Daniell (Fig. S3), Rimae Goclenius (Fig. S15), and Rima Cauchy (Fig. S2) and many other graben that were not included in our detailed topographic assessment (Fig. 2B). After emplacement of the mare units, they must have cooled and contracted (Melosh et al., 2013), placing these units in an extensional stress state. Mechanically weaker zones, such as the mare-highland transitions, served as areas where faults localized.

The intrusion of dikes and topographic adjustment to mare loading of basins likely were additional factors contributing to the formation of lunar graben and thus may have acted in concert or succession with mare cooling. It has been proposed that igneous dikes at depth are required to form lunar graben (Head and Wilson, 1993; Wilson et al., 2011; Klimczak, 2014). The dikes are likely correlated with the length of the graben and may have stalled at depths as shallow as 100–500 m from the lunar surface (Klimczak, 2014). In order for igneous dikes to form, the lunar lithosphere would also have to be under extension, and thus this tectonic regime is conducive to both dike and graben formation. Based on the methodology used here, we cannot distinguish between graben formation with or without dike intrusion, as both processes have the potential to produce all of the geomorphologic characteristics of normal faults described in this study. Further research comparing dike-related topography, dike dimensions, and fault slip distributions would allow us to further distinguish the formation mechanisms of the lunar graben.

CONCLUSIONS

We mapped the extent of lunar graben surrounding the maria and analyzed topographic variations of 14 lunar graben that consist of 184 individual fault segments. We constructed structural maps, derived fault-slip distributions, and performed displacement-to-length scaling and overlap-to-spacing analyses on the faults considered in this study. Our results show that displacement scales disproportionately with length for graben on the Moon and that slip distributions first and foremost reflect fault interaction between fault segments of the graben.

Individual slip distributions in this study revealed peaked displacement reflecting uninhibited growth of fault systems, skewed displacement

that highlights fault linkage, and plateaued slip distributions that may suggest a mechanical restriction at depth. Additionally, we found that three graben systems have substantially higher displacements than the other 11 graben systems, which we attribute to differences in mechanical properties, such as thickness of mechanical units or degree of fracturing between the anorthositic highlands and the basaltic maria. Graben symmetry displays several stages of maturity, where some graben have not reached full symmetry.

Our study presents an in-depth investigation of long lunar graben that brings new insights for their fault scaling relationships. D_{\max}/L scaling shows that the ratio for individual faults is higher (0.012) than the ratio for the cumulative graben population (0.0023). The best-fit power-law relationship for the cumulative graben is $D_{\max} = 0.171L^{0.64}$. These relationships point to various stages of fault interaction and linkage and show that lunar normal faults have lower displacements when compared to equally long terrestrial faults. However, normal faults on the Moon have higher D_{\max}/L ratios than previously predicted from modeling (Schultz et al., 2006), and results also reveal a relationship between displacement and terrain type. Furthermore, overlap-to-spacing ratios suggest that overlap scales to spacing by multiples of 5–6. These statistics do not help us understand how many normal fault populations are present on the Moon, and thus they cannot be used to distinguish between different tectonic processes responsible for graben formation. However, information from displacement paired with map patterns shows that long lunar graben are either concentric or radial to the maria, where mare-concentric grabens, in particular, show the master fault dipping toward the mare center. Therefore, we infer that formation of these graben was linked to cooling of the lunar maria.

In the future, our results can be used to better understand fault growth mechanisms on the Moon, as well as to better constrain mechanical properties of various types of host rock on the Moon. The data set will also enable us to further investigate the relationships among graben orientation, normal fault morphology, and the presence or absence of underlying dikes.

ACKNOWLEDGMENTS

We thank Science Editor Kurt Stuewe and two anonymous reviewers for their constructive comments on this research. This work was supported by the Lunar Data Analysis Program under grant NNX15AP91G.

REFERENCES CITED

- Arthur, D.W.G., Agniray, A.P., Horvath, R.A., Wood, C.A., and Chapman, C.R., 1963, The system of lunar craters, quadrants: I, II, III, IV: *Communications of the Lunar and Planetary Laboratory*, v. 2, p. 1–81.
- Cartwright, J.A., Trudgill, B.D., and Mansfield, C.S., 1995, Fault growth by segment linkage: An explanation for scatter in maximum displacement and trace length data from the Canyonlands grabens of SE Utah: *Journal of Structural Geology*, v. 17, p. 1319–1326, [https://doi.org/10.1016/0191-8141\(95\)00033-A](https://doi.org/10.1016/0191-8141(95)00033-A).
- Clark, R.M., and Cox, S., 1996, A modern regression approach to determining fault displacement-length scaling relationships: *Journal of Structural Geology*, v. 18, p. 147–152, [https://doi.org/10.1016/S0191-8141\(96\)80040-X](https://doi.org/10.1016/S0191-8141(96)80040-X).
- Cowie, P.A., and Scholz, C.H., 1992a, Displacement length scaling relationship for faults—Data synthesis and discussion: *Journal of Structural Geology*, v. 14, p. 1149–1156, [https://doi.org/10.1016/0191-8141\(92\)90066-6](https://doi.org/10.1016/0191-8141(92)90066-6).
- Cowie, P.A., and Scholz, C.H., 1992b, Physical explanation for the displacement length relationship of faults using a post-yield fracture-mechanics model: *Journal of Structural Geology*, v. 14, p. 1133–1148, [https://doi.org/10.1016/0191-8141\(92\)90065-5](https://doi.org/10.1016/0191-8141(92)90065-5).
- Dawers, N.H., and Anders, M.H., 1995, Displacement-length scaling and fault linkage: *Journal of Structural Geology*, v. 17, p. 607–614, [https://doi.org/10.1016/0191-8141\(94\)00091-D](https://doi.org/10.1016/0191-8141(94)00091-D).
- Dawers, N.H., Anders, M.H., and Scholz, C.H., 1993, Growth of normal faults: Displacement-length scaling: *Geology*, v. 21, p. 1107–1110, [https://doi.org/10.1130/0091-7613\(1993\)021<1107:GONFL>2.3.CO;2](https://doi.org/10.1130/0091-7613(1993)021<1107:GONFL>2.3.CO;2).
- Fossen, H., 2009, Faults, in *Structural Geology*: Cambridge, UK, Cambridge University Press, p. 151–188, <https://doi.org/10.1017/CBO9780511777806.010>.
- Fossen, H., and Rotevatn, A., 2016, Fault linkage and relay structures in extensional settings—A review: *Earth-Science Reviews*, v. 154, p. 14–28, <https://doi.org/10.1016/j.earscirev.2015.11.014>.
- Fossen, H., Schultz, R.A., and Rundhovde, E., 2010, Fault linkage and graben stepovers in the Canyonlands (Utah) and the North Sea Viking graben, with implications for hydrocarbon migration and accumulation: *American Association of Petroleum Geologists Bulletin*, v. 94, p. 597–613, <https://doi.org/10.1306/10130909088>.
- Freed, A.M., Melosh, H.J., and Solomon, S.C., 2001, Tectonics of mascon loading: Resolution of the strike-slip faulting paradox: *Journal of Geophysical Research*, v. 106, no. E9, p. 20,603–20,620, <https://doi.org/10.1029/2000JE001347>.
- French, R.A., Bina, C.R., Robinson, M.S., and Watters, T.R., 2015, Small-scale lunar graben: Distribution, dimensions, and formation processes: *Icarus*, v. 252, p. 95–106, <https://doi.org/10.1016/j.icarus.2014.12.031>.
- Gillet, K., Margerin, L., Calvet, M., and Monnereau, M., 2017, Scattering attenuation profile of the Moon: Implications for shallow moonquakes and the structure of the megaregolith: *Physics of the Earth and Planetary Interiors*, v. 262, p. 28–40, <https://doi.org/10.1016/j.pepi.2016.11.001>.
- Golombek, M.P., 1979, Structural analysis of lunar grabens and the shallow crustal structure of the Moon: *Journal of Geophysical Research—Solid Earth*, v. 84, p. 4657–4666, <https://doi.org/10.1029/JB084iB09p04657>.
- Golombek, M.P., and McGill, G.E., 1983, Grabens, basin tectonics, and the maximum total expansion of the Moon: *Journal of Geophysical Research—Solid Earth*, v. 88, p. 3563–3578, <https://doi.org/10.1029/JB088iB04p03563>.
- Gong, S., Wieczorek, M.A., Nimmo, F., Kiefer, W.S., Head, J., Huang, C., Smith, D.E., and Zuber, M.T., 2016, Thicknesses of mare basalts on the Moon from gravity and topography: *Journal of Geophysical Research—Planets*, v. 121, p. 854–870, <https://doi.org/10.1002/2016JE005008>.
- Gudmundsson, A., De Guidi, G., and Scudero, S., 2013, Length-displacement scaling and fault growth: *Tectonophysics*, v. 608, p. 1298–1309, <https://doi.org/10.1016/j.tecto.2013.06.012>.
- Gupta, A., and Scholz, C.H., 2000, A model of normal fault interaction based on observations and theory: *Journal of Structural Geology*, v. 22, p. 865–879, [https://doi.org/10.1016/S0191-8141\(00\)00011-0](https://doi.org/10.1016/S0191-8141(00)00011-0).
- Head, J.W., and Wilson, L., 1993, Lunar graben formation due to near-surface deformation accompanying dike emplacement: *Planetary and Space Science*, v. 41, p. 719–727, [https://doi.org/10.1016/0032-0633\(93\)90114-H](https://doi.org/10.1016/0032-0633(93)90114-H).
- Hiesinger, H., and Head, J.W., 2006, New views of lunar geoscience: An introduction and overview: *Reviews in Mineralogy and Geochemistry*, v. 60, p. 1–81, <https://doi.org/10.2138/rmg.2006.60.1>.
- Jaumann, R., Hiesinger, H., Anand, M., Crawford, I.A., Wagner, R., Sohl, F., Jolliff, B.L., Scholten, F., Knapmeyer, M., Hoffmann, H., Hussmann, H., Grott, M., Hempel, S., Köhler, U., Krohn, K., Schmitz, N., Carpenter, J., Wieczorek, M., Spohn, T., Robinson, M.S., and Oberst, J., 2012, Geology, geochemistry, and geophysics of the Moon: Status of current understanding: *Planetary and Space Science*, v. 74, p. 15–41, <https://doi.org/10.1016/j.pss.2012.08.019>.
- Jozwiak, L.M., Head, J.W., Zuber, M.T., Smith, D.E., and Neumann, G.A., 2012, Lunar floor-fractured craters: Classification, distribution, origin and implications for magmatism and shallow crustal structure: *Journal of Geophysical Research—Planets*, v. 117, p. 1–23, <https://doi.org/10.1029/2012JE004134>.
- Jozwiak, L.M., Head, J.W., and Wilson, L., 2015, Lunar floor-fractured craters as magmatic intrusions: Geometry, modes of emplacement, associated tectonic and volcanic features, and implications for gravity anomalies: *Icarus*, v. 248, p. 424–447, <https://doi.org/10.1016/j.icarus.2014.10.052>.
- Kim, Y.-S., Peacock, D.C.P., and Sanderson, D.J., 2004, Fault damage zones: *Journal of Structural Geology*, v. 26, p. 503–517, <https://doi.org/10.1016/j.jsg.2003.08.002>.
- Klimczak, C., 2014, Geomorphology of lunar grabens requires igneous dikes at depth: *Geology*, v. 42, p. 963–966, <https://doi.org/10.1130/G35984.1>.
- Krantz, R.W., 1988, Multiple fault sets and three-dimensional strain: Theory and application: *Journal of Structural Geology*, v. 10, p. 225–237, [https://doi.org/10.1016/0191-8141\(88\)90056-9](https://doi.org/10.1016/0191-8141(88)90056-9).
- Long, J.J., and Imber, J., 2011, Geological controls on fault relay zone scaling: *Journal of Structural Geology*, v. 33, p. 1790–1800, <https://doi.org/10.1016/j.jsg.2011.09.011>.
- Mansfield, C., and Cartwright, J., 2001, Fault growth by linkage: Observations and implications from analogue models: *Journal of Structural Geology*, v. 23, p. 745–763, [https://doi.org/10.1016/S0191-8141\(00\)00134-6](https://doi.org/10.1016/S0191-8141(00)00134-6).
- Melosh, H.J., Freed, A.M., Johnson, B.C., Blair, D.M., Andrews-Hanna, J.C., Neumann, A.A., Phillips, R.J., Smith, D.E., Solomon, S.C., Wieczorek, M.A., and Zuber, M.T., 2013, The origin of lunar mascon basins: *Science*, v. 340, p. 1552–1555, <https://doi.org/10.1126/science.1235768>.
- Michaut, C., Thiriet, M., and Thorey, C., 2016, Insights into mare basalt thicknesses on the Moon from intrusive magmatism: *Physics of the Earth and Planetary Interiors*, v. 257, p. 187–192, <https://doi.org/10.1016/j.pepi.2016.05.019>.
- Muraoka, H., and Kamata, H., 1983, Displacement distribution along minor fault traces: *Journal of Structural Geology*, v. 5, p. 483–495, [https://doi.org/10.1016/0191-8141\(83\)90054-8](https://doi.org/10.1016/0191-8141(83)90054-8).
- Nahm, A.L., 2016, A new map of graben on the lunar nearside: Initial observations and classification, in *Proceedings of the 47th Lunar and Planetary Science Conference*: Houston, Texas, Lunar and Planetary Institute, p. 1855.
- Nahm, A.L., and Schultz, R.A., 2015, Rupes Recta and the geological history of the Mare Nubium region of the Moon: Insights from forward mechanical modelling of the “Straight Wall,” in Platz, T., Massironi, M., Byrne, P.K., and Hiesinger, H., eds., *Volcanism and Tectonism Across the Inner Solar System: Geological Society of London Special Publication 401*, p. 377–394, <https://doi.org/10.1144/SP401.4>.
- Opheim, J.A., and Gudmundsson, A., 1989, Formation and geometry of fractures, and related volcanism, of the Krafla fissure swarm, northeast Iceland: *Geological Society of America Bulletin*, v. 101, p. 1608–1622, [https://doi.org/10.1130/0016-7606\(1989\)101<1608:FAGFOA>2.3.CO;2](https://doi.org/10.1130/0016-7606(1989)101<1608:FAGFOA>2.3.CO;2).
- Peacock, D., 2002, Propagation, interaction and linkage in normal fault systems: *Earth-Science Reviews*, v. 58, p. 121–142, [https://doi.org/10.1016/S0012-8252\(01\)00085-X](https://doi.org/10.1016/S0012-8252(01)00085-X).
- Peacock, D.C.P., and Sanderson, D.J., 1991, Displacements, segment linkage and relay ramps in normal fault zones: *Journal of Structural Geology*, v. 13, p. 721–733, [https://doi.org/10.1016/0191-8141\(91\)90033-F](https://doi.org/10.1016/0191-8141(91)90033-F).
- Polit, A.T., Schultz, R.A., and Soliva, R., 2009, Geometry, displacement-length scaling, and extensional strain of normal faults on Mars with inferences on mechanical stratigraphy

- of the Martian crust: *Journal of Structural Geology*, v. 31, p. 662–673, <https://doi.org/10.1016/j.jsg.2009.03.016>.
- Roggan, L., Hetzel, R., Hiesinger, H., Clark, J.D., Hampel, A., and van der Bogert, C.H., 2017, Length-displacement scaling of thrust faults on the Moon and the formation of uphill-facing scarps: *Icarus*, v. 292, p. 111–124, <https://doi.org/10.1016/j.icarus.2016.12.034>.
- Schultz, P.H., 1976, Floor-fractured lunar craters: *The Moon*, v. 15, p. 241–273, <https://doi.org/10.1007/BF00562240>.
- Schultz, R.A., and Fossen, H., 2002, Displacement-length scaling in three dimensions: The importance of aspect ratio and application to deformation bands: *Journal of Structural Geology*, v. 24, p. 1389–1411, [https://doi.org/10.1016/S0191-8141\(01\)00146-8](https://doi.org/10.1016/S0191-8141(01)00146-8).
- Schultz, R.A., Okubo, C.H., and Wilkins, S.J., 2006, Displacement-length scaling relations for faults on the terrestrial planets: *Journal of Structural Geology*, v. 28, p. 2182–2193, <https://doi.org/10.1016/j.jsg.2006.03.034>.
- Schultz, R.A., Moore, J.M., Grosfils, E.B., Tanaka, K.L., and Mege, D., 2007, The Canyonlands model for planetary grabens: Revised physical basis and implications, in Chapman, M., ed., *The Geology of Mars: Evidence from Earth-Based Analogs*: Cambridge, UK, Cambridge University Press, p. 371–399, <https://doi.org/10.1017/CBO9780511536014.016>.
- Smith, D.E., Zuber, M.T., Jackson, G.B., Cavanaugh, J.F., Neumann, G.A., Riris, H., Sun, X., Zellar, R.S., Coltharp, C., Connally, J., Katz, R.B., Kleynner, I., Liiva, P., Matuszeski, A., Mazarico, E.M., McGarry, J.F., Novo-Gradac, A.-M., Ott, M.N., Peters, C., Ramos-Izquierdo, L.A., Ramsey, L., Rowlands, D.D., Schmidt, S., Scott, V.S., III, Shaw, G.B., Smith, J.C., Swinski, J.-P., Torrence, M.H., Unger, G., Yu, A.W., and Zagwodzki, T.W., 2010, The Lunar Orbiter Laser Altimeter investigation on the *Lunar Reconnaissance Orbiter* mission: *Space Science Reviews*, v. 150, p. 209–241, <https://doi.org/10.1007/s11214-009-9512-y>.
- Soliva, R., and Benedicto, A., 2004, A linkage criterion for segmented normal faults: *Journal of Structural Geology*, v. 26, p. 2251–2267, <https://doi.org/10.1016/j.jsg.2004.06.008>.
- Soliva, R., and Benedicto, A., 2005, Geometry, scaling relations and spacing of vertically restricted normal faults: *Journal of Structural Geology*, v. 27, p. 317–325, <https://doi.org/10.1016/j.jsg.2004.08.010>.
- Soliva, R., Schultz, R.A., Benedicto, A., and Soliva, R., 2005, Three-dimensional displacement-length scaling and maximum dimension of normal faults in layered rocks: *Geophysical Research Letters*, v. 32, L16302, <https://doi.org/10.1029/2005GL023007>.
- Soliva, R., Benedicto, A., and Maerten, L., 2006, Spacing and linkage of confined normal faults: Importance of mechanical thickness: *Journal of Geophysical Research*, v. 111, B01402, <https://doi.org/10.1029/2004JB003507>.
- Solomon, S.C., and Head, J.W., 1979, Vertical movement in mare basins: Relation to mare emplacement, basin tectonics, and lunar thermal history: *Journal of Geophysical Research*, v. 84, no. B4, p. 1667–1682, <https://doi.org/10.1029/JB084iB04p01667>.
- Thomson, B.J., Grosfils, E.B., Bussey, D.B.J., and Spudis, P.D., 2009, A new technique for estimating the thickness of mare basalts in Imbrium Basin: *Geophysical Research Letters*, v. 36, L12201, <https://doi.org/10.1029/2009GL037600>.
- Walsh, J.J., and Watterson, J., 1987, Distributions of cumulative displacement and seismic slip on a single normal fault surface: *Journal of Structural Geology*, v. 9, p. 1039–1046, [https://doi.org/10.1016/0191-8141\(87\)90012-5](https://doi.org/10.1016/0191-8141(87)90012-5).
- Walsh, J.J., Nicol, A., and Childs, C., 2002, An alternative model for the growth of faults: *Journal of Structural Geology*, v. 24, p. 1669–1675, [https://doi.org/10.1016/S0191-8141\(01\)00165-1](https://doi.org/10.1016/S0191-8141(01)00165-1).
- Watters, T.R., and Johnson, C.L., 2010, *Lunar tectonics*, in Watters, T.R., and Schultz, R.A., eds., *Planetary Tectonics*: New York, Cambridge University Press, p. 121–182.
- Watters, T.R., Schultz, R.A., and Robinson, M.S., 2000, Displacement-length relations of thrust faults associated with lobate scarps on Mercury and Mars: Comparison with terrestrial faults: *Geophysical Research Letters*, v. 27, p. 3659–3662, <https://doi.org/10.1029/2000GL011554>.
- Wieczorek, M.A., Neumann, G.A., Nimmo, F., Kiefer, W.S., Taylor, G.J., Melosh, H.J., Phillips, R.J., Solomon, S.C., Andrews-Hanna, J.C., Asmar, S.W., Konopliv, A.S., Lemoine, F.G., Smith, D.E., Watkins, M.M., Williams, J.G., and Zuber, M.T., 2013, The crust of the Moon as seen by GRAIL: *Science*, v. 339, p. 671–675, <https://doi.org/10.1126/science.1231530>.
- Wilhelms, D.E., Howard, K.A., and Wilshire, H.G., 1979, *Geologic Map of the South Side of the Moon*: U.S. Geological Survey IMAP 1162, scale 1:5,000,000.
- Willemse, E.J.M., 1997, Segmented normal faults: Correspondence between three-dimensional mechanical models and field data: *Journal of Geophysical Research—Solid Earth*, v. 102, p. 675–692, <https://doi.org/10.1029/96JB01651>.
- Willemse, E.J.M., Pollard, D.D., and Aydin, A., 1996, Three-dimensional analyses of slip distributions on normal fault arrays with consequences for fault scaling: *Journal of Structural Geology*, v. 18, p. 295–309, [https://doi.org/10.1016/S0191-8141\(96\)80051-4](https://doi.org/10.1016/S0191-8141(96)80051-4).
- Wilson, L., Hawke, B.R., Giguere, T.A., and Petrycki, E.R., 2011, An igneous origin for Rima Hyginus and Hyginus crater on the Moon: *Icarus*, v. 215, p. 584–595, <https://doi.org/10.1016/j.icarus.2011.07.003>.

MANUSCRIPT RECEIVED 3 JULY 2018

REVISED MANUSCRIPT RECEIVED 30 NOVEMBER 2018

MANUSCRIPT ACCEPTED 10 JANUARY 2019